Durham E-Theses

Scattering Microscopy in Microfluidic Channels using an External Cavity Diode Laser

RENDER, RY

How to cite:

RENDER, RY (2021) *Scattering Microscopy in Microfluidic Channels using an External Cavity Diode Laser*, Durham theses, Durham University. Available at Durham E-Theses Online: http://etheses.dur.ac.uk/14355/

Scattering Microscopy in Microfluidic Channels using an External Cavity Diode Laser

Ry Render

A thesis presented for the degree of

Master of Science via Research
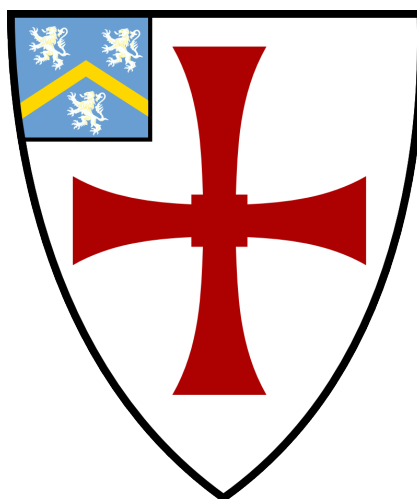
Centre for Advanced Instrumentation

The University of Durham

United Kingdom

30th September 2021

Scattering Microscopy in Microfluidic Channels using an External Cavity Diode Laser
Ry Render

Abstract

A proof of concept system for the use of an external cavity diode laser in microscopy-based measurements of scattering particles within a microfluidic channel was demonstrated. Both a highly reflective mirror of reflectivity R = 98% and a blazed reflective diffraction grating of average efficiency 60% were used to form two variations of the external cavity. Varying concentrations of an ethylene glycol based titanium oxide nanofluid were pumped with a syringe pump through a $1\mu l$ flow cell at a rate of 0.005±0.001ml per minute. Compared to a control of the system without an extended cavity, the system with the mirror demonstrated a higher performing concentration/intensity relationship, verified with a Z-value statistic test to above a 5σ confidence level compared with the control. This allows for higher precision determination of scatterer concentration, along with potentially a higher dynamic range. The blazed diffraction grating was demonstrated to have less of a benefit than the highly reflective mirror, though still demonstrated potential use cases with a higher dynamic range than the control. Exponential fits were found using χ^2 linear regression fitting, although due to reduced $\chi^2 \approx 350$, it is assumed there is an underestimation in the error of titanium oxide concentration. These results suggest that an external cavity diode laser may be an improvement compared to a standard diode laser as a way of measuring concentration of light-scattering particles, such as droplets in focused flow droplet microfluidics. Inline low concentration scatterer measuring techniques were described, with attempts being inconclusive due to CCD software limitations.

Supervisors: Prof John Girkin and Dr Kieran O'Brien

Acknowledgements

Dedication

I dedicate this thesis to my partner Lucas, whose support during these trying times gave me the love and support needed to express the level of academic ability given in this paper. I personally thank everyone at CfAI who has helped me throughout, and my friends for being constantly supportive. You're all truly wonderful.

Contents

Declaration

The work in this thesis is based on research carried out at the Centre for Advanced Instrumentation, Department of Physics, University of Durham, England. No part of this thesis has been submitted elsewhere for any other degree or qualification, and it is the sole work of the author unless referenced to the contrary in the text.

List of Figures

List of Tables

Glossary

GaAs Gallium Arsenide

ECDL External Cavity Diode Laser

CCD Charged-Couple Device

TiO$_2$ Titanium Oxide

EG Ethylene Glycol

Background and Theory

This chapter will cover the key concepts and background information required to understand the project's aims and execution. Then the key experimental designs used during the study will be outlined for the undertaking of measurements. The chapter will conclude with the objectives aimed to be satisfied by the study.

Semiconducting Laser Diodes

Semiconductor lasers are a type of laser that utilise solid-state gain medium. Gain occurs with the utilisation of a transition between two energy bands with a high density of charge carriers within the conduction band. Although there are different types of semiconductor lasers, diode lasers are the most commonly used type within both societal and laboratory settings. They are known to be cheap to produce and can have high electrical to optical power efficiency [1]. This makes diode lasers ideal for applications where their relatively low power is not a limiting factor, such as in spectroscopy or optical communications. Further examples of their use include, but are not limited to, the detection of gravitational waves [2] and their use as an optical pump in other laser systems [3].

Diode lasers generate gain using either a p-n or p-i-n junction. As electron-hole pairs meet, the annihilation of the pair produces a photon with the surplus energy. This process can be spontaneous or stimulated, with spontaneous emission being a

---
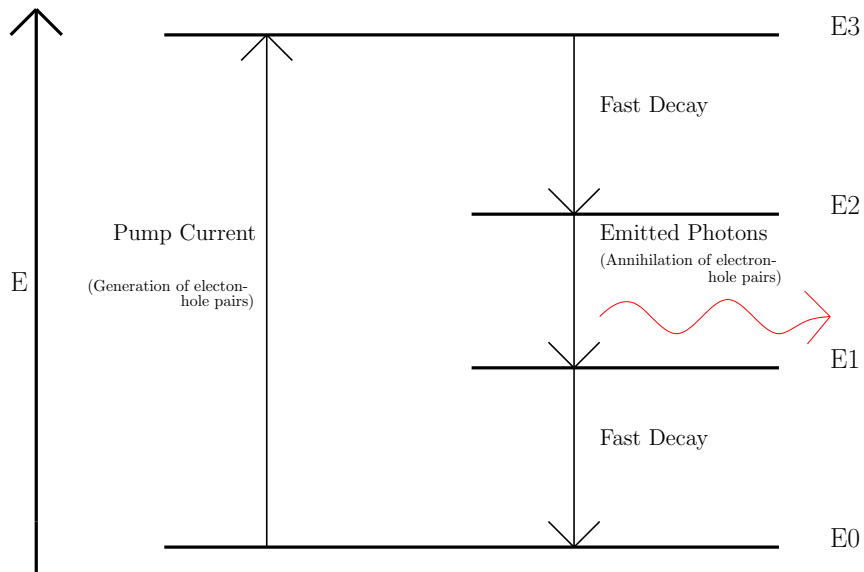
Figure 1.1: Energy level diagram showing a simplified version of the operation of laser-diode gain.

random quantum process and stimulated emission being produced by interaction with photons.

This regime utilises a four energy level system, but unlike other solid state lasers or gas lasers, the processes which lead to optical gain are complicated due to many possible interactions between the photons and the electron-hole pairs. The energy level diagram in Figure 1.1 shows a simplified version of these processes.

The current through the laser diode acts as a pump, generating electron-hole pairs, raising the electrons to energy level 3, which then undergoes a fast decay to energy level 2. The electron-hole pair is annihilated as the electron drops to energy level 1, producing the aforementioned photon which contributes to lasing, after which the electron undergoes another fast decay to the ground energy state level 0, where the process begins again. By using a laser resonator setup, the spontaneous emission can be used to produce further stimulated emission. When photons circulate through the semiconductor gain material, they contribute to the rate at which electron-hole pairs annihilate, stimulating the electron to move from level 2 to level 1. The photons then eventually decay from the system via emission from the partially reflective mirror, which produces the output beam of the laser.

For any lasing to occur, the round trip gain of photons within the resonator must exceed the round trip losses. Usually, this is performed by the use of a highly reflective mirror and a partially reflective mirror. With Gallium Arsenide (GaAs) semiconductors however, the natural cleaving of the material can form a cavity. Assuming a refractive index of $\eta = 3.6$, the reflectivity at a GaAs boundary can be calculated using:

$$R = (\frac{\eta - 1}{\eta + 1})^2 \tag{1.1}$$

Which then is calculated as:

$$R = (\frac{2.6}{4.6})^2 \approx 0.32 \tag{1.2}$$

This is confirmed by using the appropriate figures from [4], with light approximately in the 800nm range. It can then be shown by using this approximate value for the reflectivity that the cavity has low finesse. Finesse is an indirect measure of how many round trips a photon will make and is given by:

$$F = (\frac{\pi \sqrt{R}}{1 - R}) \tag{1.3}$$

With an estimated reflectivity of 32%, the finesse is shown to be:

$$(\frac{\pi \sqrt{0.32}}{0.68})^2 \approx 2.6 \tag{1.4}$$

This low finesse cavity along with the particularly high level of optical gain allows the diode laser to operate without the use of additional reflective elements. One consequence of increasing the finesse, is not only an increase of the round trips of the photons, but also an increase of the ratio between the free spectral range and the full width at half maximum. This means that not only does the power output increase, but also the photons are concentrated at specific wavelengths. Therefore, it is of interest to increase the finesse, which can be done by adding an optical element with a higher reflectivity.

The External Cavity Diode Laser

With the addition of optics outside of the diode laser, an external cavity can be formed, feeding light back into the cavity and therefore back through the gain medium. This setup is known as an External Cavity Diode Laser (ECDL). With the addition of the external cavity, the ECDL is now subject to the effects of the external cavity, as well as to the effects of the internal cavity. Due to the internal cavity being small, the full width half maximum of the peaks will be a significant proportion of the free spectral range of the laser diode gain. This means that to limit the linewidth of the output, the internal cavity effects would ideally be removed. Realistically, these effects can be reduced, but not entirely removed, by the use of an anti-reflective coating. By aligning the external cavity modes (usually achieved with a piezoelectric crystal device), the internal cavity modes (by controlling the temperature of the laser diode) and potentially a wavelength-selective element such as a reflective diffraction grating, a single frequency mode can be selected and tuned, with a low linewidth. Figure 1.2 shows how the alignment of cavity effects and the use of a diffraction grating can produce single longitudinal mode operation with an ECDL.
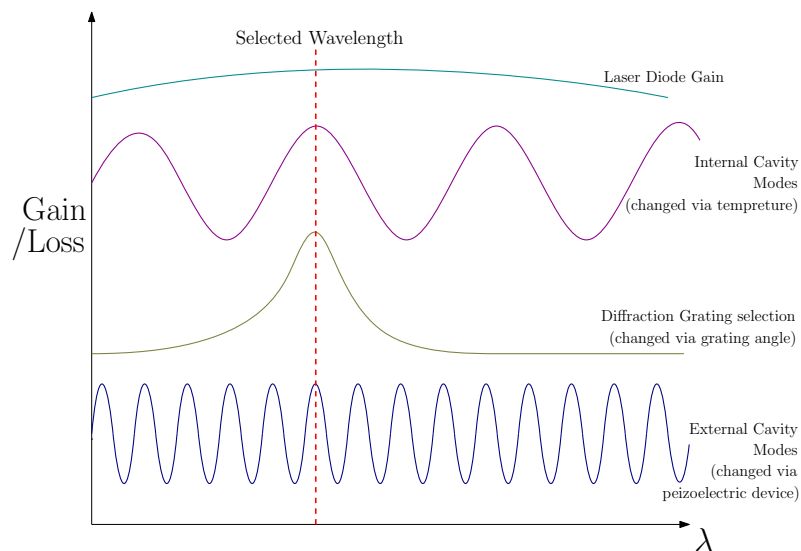
Figure 1.2: Graph showing the relative gain/loss of each element of the ECDL. The dotted red line shows how a single wavelength is isolated by adjusting for the temperature, external cavity length and diffraction grating angle.

The ECDL has another unique property allowing it to have a unique role in absorption spectroscopy and microscopy applications - the easily accessible, open cavity. This allows targets to be placed within the cavity instead of using the output beam, allowing for an effective increase in the absorption sensitivity of the target.

Light attenuation and its role in measurement

When light interacts with matter, there are several outcomes which can occur, from scattering effects to absorption. Both of these are types of light attenuation.

Absorption

Absorption usually occurs between an electron in an atom or molecular bond and a photon. The photon's energy is absorbed by the electron, changing the electron's energy level. While this may cause a change to the sample chemically, the effect this has to the measured output of a beam is a relative decrease in light from that area of the sample, as the photon is no longer received at the detector.

Beer-Lambert Law

A description for the behaviour of absorption of light is given by the Beer-Lambert law.

The Beer-Lambert law states that the absorbance of a material is proportional to the optical path length of light through the attenuating media and proportional to the concentration of the attenuating media. There are multiple ways of writing the Beer-Lambert law mathematically, but for the purposes of this study it will be written using the form from [5]:

$$I_T(\omega) = I_0 \exp[-\alpha(\omega)l] \tag{1.5}$$

where $I_T(\omega)$ is the transmitted light intensity for a given frequency, I_0 is the initial light intensity, $-\alpha(\omega)$ is the absorption coefficient for the material for a given

frequency and l is the total optical path length through the material.

Absorption is an important aspect in both spectroscopy and microscopy. In spectroscopy, absorption of a particular wavelength of light is analysed via the investigation of 'troughs' in the spectral intensity profile at a given wavelength, which can be used to determine relative concentrations through the Beer-Lambert law and a suitable calibration curve for a specific analyte. In particular [6] showed a significantly high sensitivity in the detection of absorbing material in the parts per billion (ppb) to parts per trillion (ppt) range. In microscopy, since many samples are damaged through their interactions with light, it is often preferable to have low intensity illumination methods. Through the use of an ECDL, it has been shown that by passing the light through the sample multiple times, there is an effective increase in absorbance [7]. This leads to increase the contrast of the image due to the increased effective optical path length, allowing the ECDL's output beam to be used as a microscope.

Scattering

Along with absorption, one of the most common optical phenomena in the field of microscopy is scattering. Similar to the case of absorption, Rayleigh scattering occurs when a photon interacts with a particle of much smaller size compared to the photon's wavelength, with a photon of the same wavelength being emitted in a different path. When the wavelength is similar to the size of the particle, the scattering observed is instead Mie scattering [8], with the majority of the photons having a similar path to the original. This type of scattering is known as elastic scattering as the energy of the photon does not change, and is the types of scattering which will be the focus of this study.

In most circumstances, scattering is considered an effect to be compensated for in the field of microscopy as it alters the photon's trajectory, spatially separating intensities in a manner which reduces image quality. There are, however, uses for scattering in microscopy, and in a similar manner to absorption, the Beer-Lambert

law can be used to determine the concentration of scattering particles in a sample. In a similar manner to how absorption measurements have been observed to have a high level of precision with an ECDL, the same may be possible with regards to scattering.

In the case of Mie scattering, P L Gourley [9] finds a similar relationship to that of the Beer-Lambert law with regards to the attenuation of light:

$$I_T = I_0 \exp[-\mu l] \tag{1.6}$$

where I_T is the transmitted light intensity for a given frequency, I_0 is the initial light intensity, l is the total optical path length through the material and μ is the scattering for the material given by:

$$\mu = Nk\pi r^2 \tag{1.7}$$

where N is the concentration of scattering particles, K is a cross-section which is dependent on both wavelength of light and particle diameter and r is the diameter of the particle.

For Rayleigh scattering, Gourley [9] then describes an intensity relationship which differs from the form given by the Beer-Lambert law, given as follows:

$$I_T = I_0 (\frac{16\pi^3 cM}{N_A \lambda^4})(\frac{dn}{dc})^2 \tag{1.8}$$

where I_T is the transmitted light intensity for a given frequency, I_0 is the initial light intensity, where c is the concentration of scattering particles, M is the molecular mass, N_A is Avogadro's number, λ is the wavelength of light and $\frac{dn}{dc}$ is the specific refractive increment.

Cavity effects from scattering

When a sample is placed within an external cavity it can be a source of scattering. Depending on the type of sample within the cavity, different scattering effects will take place. With low levels of absorbent molecules in solution, there is little mode

competition [10]. For larger objects in the solution, such as large organelles in a biological sample, Mie scattering and scattering due to membrane surface roughness becomes dominant. Mie scattering in particular has a larger proportion of the scattered light close to the original direction of propagation. Because of this, these cases can produce cavity resonance effects, as they tend to be scattered by a small angle, causing spectral peaks depending on the spatial and chemical characteristics of the cell [7] [9].

When light passes through a group of scattering particles, a proportion of the light which interacts with the scattering particles remains on axis. As the number of passes increases, the probability of the photon being scattered off axis increases. Depending on whether the scattering is Rayleigh dominated or Mie dominated, there can be a similar relationship to the Beer-Lambert law in each case, as shown in Equations 1.6 and 1.8. With the results provided by [6] in mind, it could be argued that the ECDL could have potential use in sensitive detection of scattering particles. As the light is attenuated in the cavity by scattering, the finesse of the cavity decreases, leading to a drop in the power output of the cavity.

In particular, the use case of microfluidic channels can involve the monitoring of the concentration of scattering particles as they travel through the system, which gives a novel target for the ECDL to investigate.

Microfluidic channels as a target

Previous studies have investigated placing absorbing samples within the cavity [6], though the use of miniature flow cells is of particular interest, as they can be used to simulate the microfluidic channels used within chemical manufacturing and pharmaceutical industries [11]. Given their size, they are ideal for controlling chemical reactions via laminar flow and provide a confined area for microscopic or spectroscopic techniques. There are many use cases of microfluidic channels.

One popular use is using microfluidic channels as miniature bioreactors, either as case studies for larger bioreactors or with many in parallel where larger reactors

are not necessary. Microscopy and spectroscopy are important in this use case as trace compounds may end up being hazardous within the manufacturing process or the final product. A similar use for microfluidic channels is in flow cytometry, where cellular samples are passed through the channel to characterise them one at a time via use of spectroscopic, fluorescence and absorbance measurements. It has already been shown that microscopic images can be produced by flowing blood cells through the cavity, with the cells' geometry contributing to the modes they produce [7].

Another common application of microfluidic channels is as focused flow droplet generators, which are used to produce emulsions of small droplets. Focused flow droplet generators function by pumping two immiscible fluids towards a common junction. One of the fluids, known as the continuous phase, is the medium in which the other fluid, the dispersed phase, forms droplets in. At the junction there is a nozzle which focuses the dispersed phase as shown in Figure 1.3
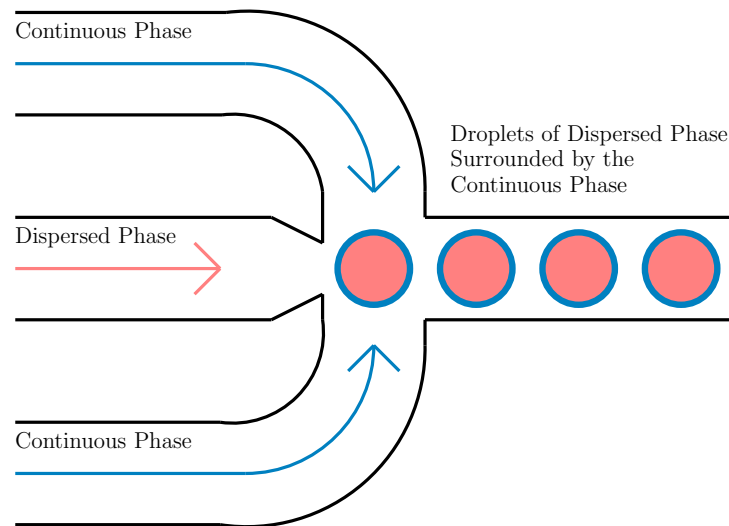
Figure 1.3: Diagram showing the main junction in a focused flow droplet generator.

This takes advantage of the liquids being immiscible and instead causes the channel in the centre to produce droplets, whose size are based on the viscosity of the fluids, their miscibility, the flow rates of both fluids and the specific material prop-

erties of the channels being used [12]. As these two fluids will often have differing refractive indices, they will induce scattering at the boundary of the two, with the magnitude of the scattering depending on the difference between indices. Because these droplets will be of relatively similar size, their respective scattering due to one droplet will be similar to that of all other droplets. It may be possible then to determine, based on the level of scattering, how many droplets there are.

These examples present an interesting use case of the ECDL's cavity for use in microscopy of microfluidic channels, particularly with focused flow droplet generators.

ECDL configurations

ECDLs do not have a monolithic design, meaning there are many possible configurations. This means that a specific experimental setup will be needed depending on the measurements planned to be taken. Some elements however are required. Since laser diodes are often small, there will be a significant amount of beam divergence as the light leaves the internal cavity, meaning that a lens must be used to collimate the light. Furthermore, the use of the laser diode's internal photodiode can become problematic when an external cavity is introduced. This is due to potential saturation of the internal photodiode which leads to loss of data, causing the readout to be inaccurate. To counteract this the use of some form of photodetection should be used externally to measure the output intensity of the beam. Two relevant ECDL configurations will be discussed below.

One of the common configurations, known as the Littrow configuration [13], uses a diffraction grating to reflect some of the light back into the cavity. The diffraction grating disperses the frequencies of the light spatially, meaning photons of a particular frequency band are reflected back into the cavity. Usually the 1st order is chosen to be reflected back into the cavity, with the 0th order being used as the output. The 1st order is chosen as it is the order with the greatest intensity; by using this order to form the extended cavity, the average number of round trips of the photons in the cavity increases, increasing the gain and further increasing

the output. This particular setup leads to a lower laser linewidth, allowing the output of the external cavity to have a larger proportion of photons at the desired frequency. The undesired frequencies are filtered out as only the photons with wavelengths sufficiently aligned with the axis will remain in the cavity. Combined with the ability to easily adjust the angle of the grating to change the frequencies selected for, a piezoelectric crystal can used to make adjustments to the cavity length, which gives both tunability and a narrow bandwidth. An initial setup using a diffraction grating is shown in Figure 1.4.
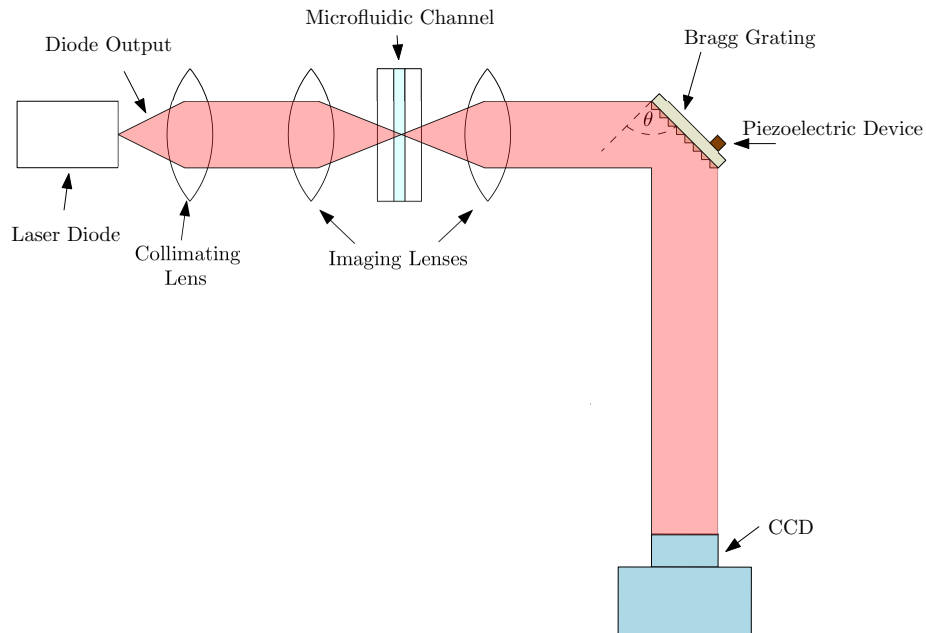
Figure 1.4: Experimental setup using a diffraction grating at angle θ with respect to the initial direction of the beam.
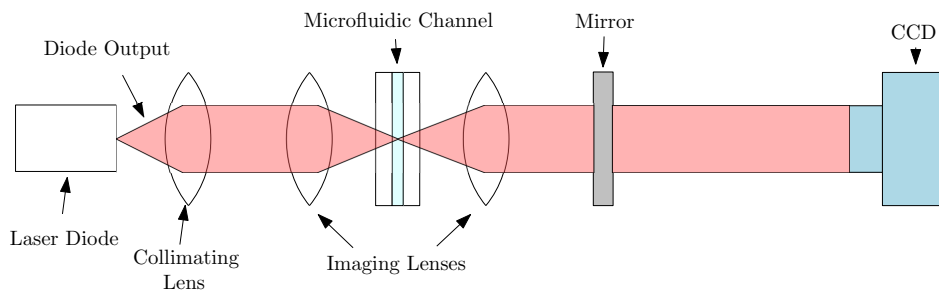
Figure 1.5: Experimental setup using a highly reflective mirror.

If we instead replace the diffraction grating with a highly reflective mirror, we can reduce the losses from the dispersing element in exchange for reduced tunability and increased linewidth. With fewer photons lost, this allows for greater sensitivity for attenuation measurements in implementations where a larger linewidth is not a limiting factor. An example of an experimental arrangement for this is given in Figure 1.5.

The configurations described will be used with a Charged-Couple Device (CCD), and potentially a photodetector. The CCD will be used to monitor the output of the beam, which will be of interest for using the ECDL as a microscope. Alongside the microfluidic channels are two imaging lenses used to focus the beam so that it images the channel and then expanded so that it can be of suitable size for the CCD and any photodetectors used. Combinations of 50:50 beamsplitters can be used to split the beams so that it can be fed into further detectors if required, with a corresponding halving of intensity.

Measurements and experiment criteria

For summary purposes, it is important to detail the scope of the study given the background provided in this chapter. The aim will be to use the proposed system designs to take measurements of intensity for varying concentrations of scattering particles. For an advantage to be demonstrated, the system will be compared with a control version of the setup, described below.

The reflective element will be removed for the system described by Figure 1.5 to remove the extended cavity. It is however difficult to draw conclusions doing the same for the system described by Figure 1.4 due to the diffraction grating's unique effects on the cavity. While the set up described by Figure 1.4 does not have a direct comparison, it will still prove useful to compare it to the 'mirrorless' set up to demonstrate benefits due to the higher finesse.

These changes ensure that all other elements of the system will be as consistent

as possible and allows for the comparison of an ECDL setup with a standard laser diode, both when lasing and when operating in LED mode.

Before each set of measurements, the threshold current will be estimated for a given alignment, so that the offset current from threshold is known, along with emphasis placed on having as similar threshold currents for each set of measurements as possible. This will be to prevent any significant increases in linewidth broadening [9] due to changes in cavity temperature which could be caused by a differing current value.

Methodology

This chapter will begin with the description of key methodological choices used within the study along with their justifications. Then the experimental apparatus used will be described along with details on the measuring equipment used. To conclude, there will be a description of statistical methods used to determine the validity of measurements and their uncertainties.

Determination of Threshold Current

With the addition of an external cavity, there is a decrease in the threshold current required for the diode to switch from acting as an LED to lasing. Because of this, a methodology for the determination of the threshold current is required for each set of measurements as small changes in the cavity alignment caused by the environment can have a significant impact on the cavity efficiency and therefore, threshold current. There are many methods of determining threshold current, all with advantages and disadvantages. Because of this, each method should be chosen based on the use case, such as the required precision and the frequency of measurements. Another important factor to consider is that once a method has been chosen, the same method must be applied to all other determinations, as it has been shown that different techniques can provide differing values for threshold current, even when the uncertainties are accounted for [14].

To determine threshold current, estimation of the first and second derivatives of the power/current curves was considered [15], although calculating these using the backwards finite difference method [16] would require evenly spaced data points. This is particularly difficult for current which is controlled on the diode controller via a continuous dial rather than a discrete one. In comparison, a two-segment fit was used to demonstrate a method which would not require evenly spaced data points. A two-segment fit partitions the data into two separate linear regression fits as below and above threshold there are separate linear relationships. By evaluating the current value where the two lines of best fit cross, an estimate of the current can be made. The partitions are chosen via manual inspection.

An example of data collected via manual input of current into the diode controller is presented in Figure 2.1, with the corresponding threshold current values and their uncertainties given in Table 2.1.
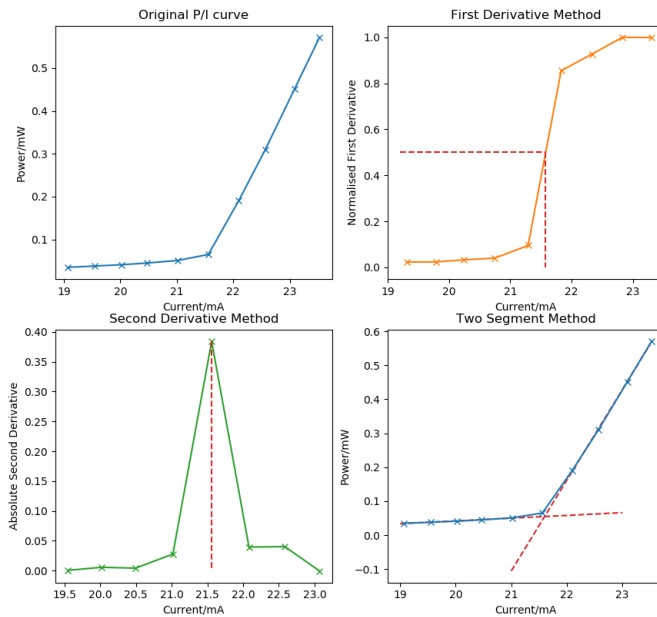
Figure 2.1: Graphs depicting the first derivative, second derivative and two-line segment methods for estimation of threshold current. The red dotted lines demonstrate how threshold current is determined in each case.

Example Threshold Current per Methodology		
Method	Estimated Current (mA)	Estimated Uncertainty (mA)
Two-segment Fit	21.6	±0.3
First Derivative	21.5	±0.9
Second Derivative	21.6	±1.4

Table 2.1: Table of threshold current values with the three described estimation methods, along with their uncertainties.

If this data could be taken with a different experimental setup allowing for automated data collection, the first derivative or second derivative techniques may be appropriate. However, due to the difference in the current values being large, there is a large error when using the method of finite difference. This is due to the error scaling in the form $O(h^2)$. O represents the truncated terms of a Taylor series which are omitted as per the finite difference approximation, with h being the distance between the data points [16]. It is important to note that the uncertainty due to the precision of the measuring equipment was omitted from this error analysis in the first and second derivative example to simplify the calculation as the error due to the precision was above an order of magnitude in difference, meaning that it would not have changed the uncertainties presented due to the singular significant figure being quoted due to the sample size [17].

Given that threshold current estimation is only needed so that an offset current above that can be used, the potential precision of these methods at lower current gaps is not required, with the two-segmented fit providing a suitable value of threshold current to work from.

Choice of Photo-detector

To measure the intensity, two methods were considered. The first method is to place a photodiode after the 50:50 beamsplitter to measure the beam concurrently with the images taken with the CCD. This however requires a method of synchronising each image taken with the CCD with a given reading from the photodiode. The second method, and the one which was used, is to derive an intensity value from

the images themselves.

This is justified as each pixel of a CCD acts as a photodiode, with the CCD constituting an array of photodiodes. For each image produced, an equivalent pixel intensity histogram can be produced. An example of this is shown in Figure 2.2.
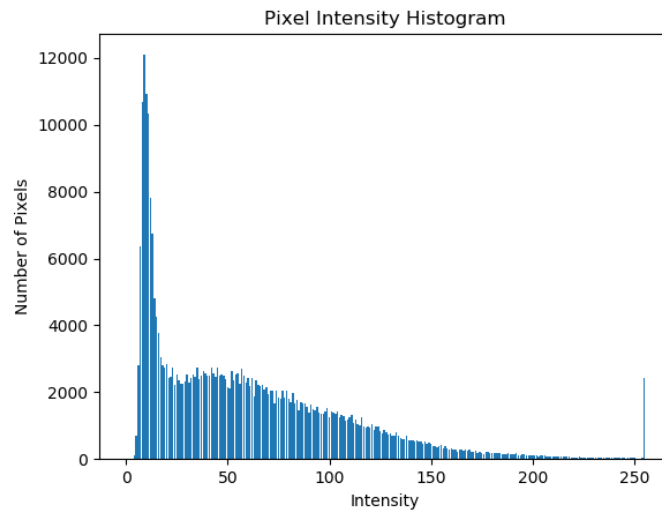
Figure 2.2: Example of a pixel histogram for an image taken during calibration.

By taking the product of the number of pixels and their respective values and summing them, a relative intensity value can be produced. This intensity value can either be converted using the CCD manufacturer's specifications to calculate a specific intensity value, but since the CCD in this study will be consistent, this is not required and so the relative intensity values will be used.

The disadvantage of this methodology is that of the CCD's limited maximum photon count per pixel, meaning that the output power of the ECDL needs to be minimized so that the maximum power the pixels on the CCD can measure is not exceeded (meaning the CCD is not saturated). Figure 2.2 demonstrates this, as there is a disproportionate increase in the number of pixels with maximum value. This limits the number of pixels which will reach saturation, as saturated pixels no longer provide further information on the intensity of light at that location. A

possible way to circumvent this is by the use of neutral density filters to sample the distribution at a lower intensity, which can then be used to map the saturated pixels to their corresponding values above the saturation limit.

Another disadvantage is the computing performance and time requirements to process the images. For example, an inefficient python program to read and convert six hundred 659x493 pixel, 8 bit images using an Intel Core i7 7700HQ at 3500 MHz clock speed was used to produce intensity values. The code finished in 34±1 seconds when utilizing all four CPU cores. With respect to the aim stated in the first chapter, the ideal use case within pharmaceutical production would require both cheap and inline uses, due to many microfluidic channels being used in parallel. Therefore this type of data collection may not be suitable in that use case, especially as the computing requirements will scale linearly with the addition of more images as shown in Figure 2.3.
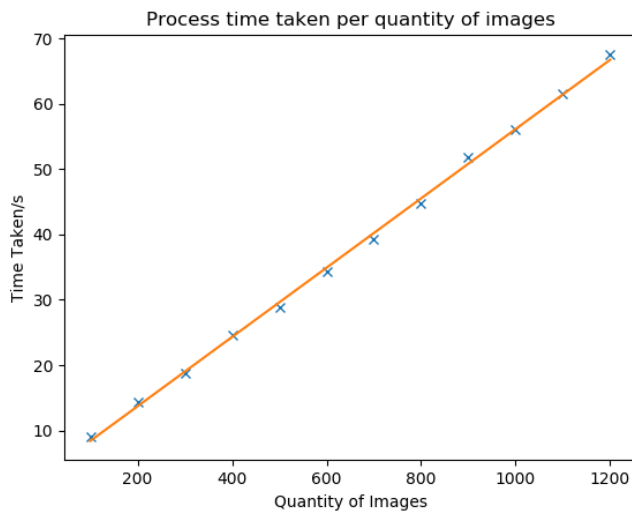
Figure 2.3: Graph demonstrating the linear relationship of image quantity and time taken to determine intensity using a Python 3.7 program.

This can be avoided by using a separate photodiode as mentioned previously, but for the verification of increased performance of the ECDL compared to a standard beam, this consideration is not necessary, although important to note.

Experimental Setup

Table 2.2 contains the list of equipment used in the experimental setup. Various mounting equipment were omitted for brevity as they were deemed unimportant for detailing the setup in terms of future reproducibility. The Figures 2.4 and 2.5 show images of the setups with respective axes labelled with respect to the explanations given for the orientation of equipment.

Equipment List			
Equipment Name	Manufacturer Name	Serial Number	Label
Laser Diode (LD)	Thorlabs	L808P030	1
LD Mount	Thorlabs	LDM21	1
LD Current Controller	Thorlabs	LDC202C	8
LD Temperature Controller	Thorlabs	TED200C	9
Collimating Lens Mount	Thorlabs	S1TM091	2
Collimating Lens	Thorlabs	C390TME-B	2
2x Triplet Lenses	Melles Griot	No longer available	3
Near IR Mirror	LaserOptik GmbH	R=98%, 850nm	5
Blazed Reflective Grating	Thorlabs	GR25-1208	5
CCD	Allied Vision	GC650	6
Syringe Pump	New Era Pump Systems, Inc	NE-300	
Syringes	BD	BD Plastipak 1ml	
Microfluidic Chip Holder	Micronit	Fluidic Connect Pro	4
Microfludic Flow Cell	Micronit	FLC50.3	4
Tubing & Connectors	Micronit	Connection Kit	7
TiO$_2$ Brookite-Nanopowder	Sigma-Aldrich	791326	
Ethylene Glycol	Aldrich	102466	
Ultrasonic Processor	Sonics & Materials, Inc	CV18	
Ultrasonic Bath	VWR	USC-TH	

Table 2.2: Table detailing the equipment used in the described setup and in the collection of data for the study.

A Thorlabs L808P030 808nm laser diode was mounted in a Thorlabs LDM21 mount. To provide control to the operational current and to lock/measure the temperature, the laser diode was then connected to the Thorlabs LDC202C and TED200C which are current and temperature controllers respectively. The diode's mount was secured to a M6 tapped breadboard so that the system could be moved to a laminar flow isolation optics bench and/or into an optically dark enclosure as required. Both of the diode controllers were placed on the same bench or enclosures as the breadboard itself.

Two triplet diode lenses (coated for 810nm, effective focal length = 12.5mm, back focal length = 6.5mm) were secured with a 3D-printed push fitting, secured to two separate lens mounts, with the second lens mount allowing for fine adjustment in the X-Y plane. Due to the asymmetry of these lenses, the larger cavity was orientated to face outside of the region being imaged, so that the initial beam of the laser diode could enter the lenses with minimal light lost. The first lens mount was then fixed to the breadboard. Because fine adjustments were needed to ensure that the light leaving the second lens would be fully collimated, the second lens mount was secured to a further translation stage (in the Z direction) which was then bolted to the breadboard.

The microfluidic chip holder was mounted on an X-Y-Z translation stage to allow for a full range of movement about the focus of the two diode lenses.

Further in the Z direction either a highly reflective near-infrared (NIR) mirror or blazed-reflective grating were placed, both attached to suitable tip-tilt mounts which allowed for calibration of optical alignment. The highly reflective mirror was placed perpendicular to the Z direction (and therefore, the direction of the beam), while the grating was placed at an angle which allowed for the desired diffraction order to be reflected into the diode. Then the CCD was mounted in one of two locations, depending on whether the measurement was using the mirror (or no reflective element) or the grating with the 1st order forming the external cavity.

Figures 2.4 and 2.5 show these configurations with labels described in Table 2.2,

with items which are mounted together given the same label and any unlabeled equipment being miscellaneous optomechanics used for alignment of optics.
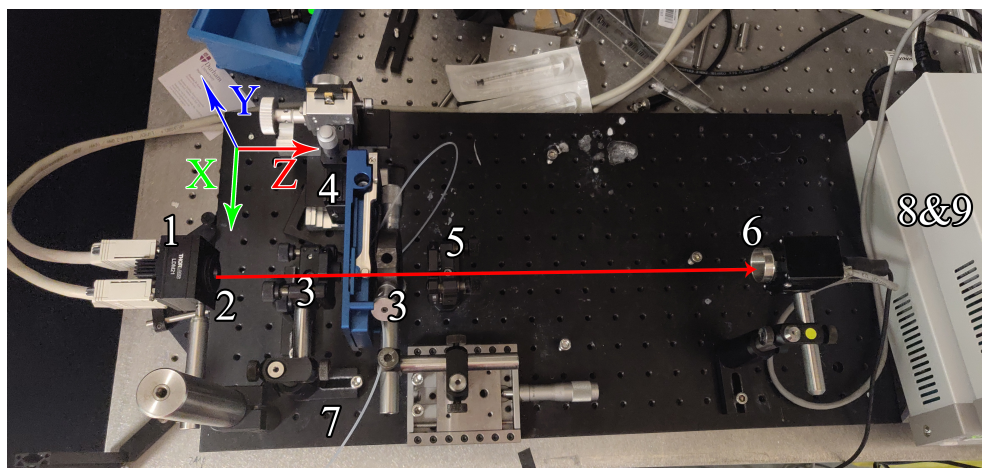
Figure 2.4: Photographic image of the setup using the highly reflective mirror, with the X-Y-Z axes labelled along with the equipment.
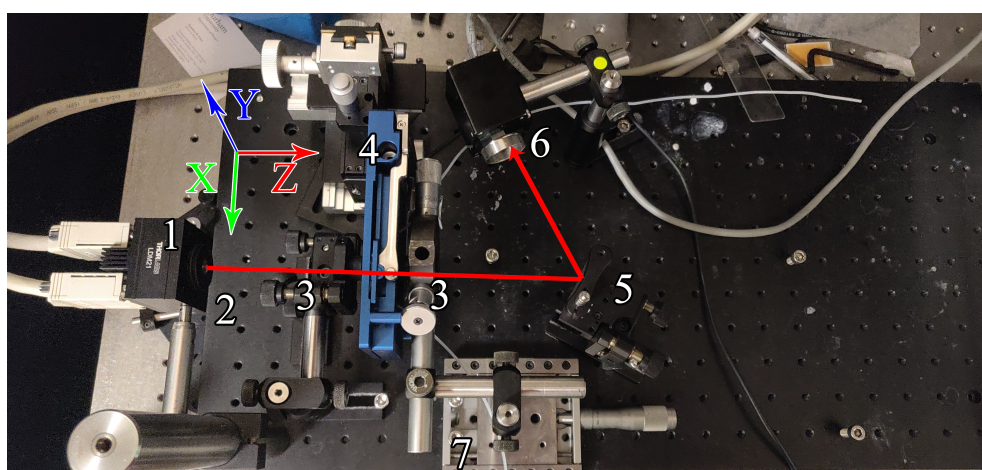
Figure 2.5: Photographic image of the setup using the blazed diffraction grating, with the X-Y-Z axes labelled, along with the equipment.

Choice of Microfluidic chip

Due to the complex topology of focused-flow microfluidic chips, they require a high level of expertise to operate. For a simplified model for use in this study, a flow cell using a singular channel containing a scattering solution was used.

The flow cell chosen was a standard Micronit 'Thin-bottomed flow cell' (FLC50.3), which was placed in a 'Fluidic Connect Pro chip holder - topconnect', with ETFE

tubing connected securely with the fittings provided in the micronit connection kit. The tubing was then connected to 1ml BD syringes which were locked in place in a NE-300 New Era Pump Systems, Inc. syringe pump, allowing for the pump rates between 0.73μl/hour to 1500ml/hour. The syringe pumps were placed on an bench external to the location that the breadboard was located on to prevent any tremors caused by the piston affecting the cavity, due to the cavity's high sensitivity to the environment.

Preparation of a Titanium Oxide Nanofluid

A solution of 'Titanium (IV) oxide, brookite - nanopowder', manufactured by Sigma-Aldrich, was used as a source of scattering particles. Titanium Oxide (TiO_2) is widely used as a scatterer due to its high refractive index [18] and low toxicity [19]. The TiO_2 mean particle size was rated less than 100nm via a scanning electron microscope. Since the mean operating wavelength of the diode is rated at 808nm, this suggests that the predominant scattering may be Rayleigh scattering over Mie scattering. Mixing the TiO_2 with a base fluid such as water or Ethylene Glycol (EG) is not sufficient for producing a mixture with a stable and homogeneous diffusion of TiO_2. Without a stable, homogeneous distribution, the TiO_2 particles will agglomerate, leading to a differing concentration as the particles clump together [20]. This would be problematic for the accurate measuring and variation of the concentration for the purposes of this experiment. Instead, a nanofluid of TiO_2 must be formed, which allows for the TiO_2 to be evenly distributed and preventing agglomeration. Both the TiO_2 and EG were measured by weight, using approximately 5.5-6.0 ml of EG as a base so there would be an excess for multiple experiments. Then for each volumetric concentration ϕ used, the required mass of TiO_2 was calculated using the equation presented in [21]:

$$\phi = \left[\frac{\frac{W_{TiO_2}}{\rho_{TiO_2}}}{\frac{W_{TiO_2}}{\rho_{TiO_2}} + \frac{W_{EG}}{\rho_{EG}}} \right] \tag{2.1}$$

where W is the weight and ρ is the density of TiO_2 and EG respectively.

To produce a nanofluid of TiO_2 and a base fluid, an ultrasonic probe was used to break up the initial sedimentation, then the mixture was agitatted in an ultrasonic bath was used as suggested by [22], operated at a frequency above 40kHz. This agitation lasted approximately 5 hours. The stability of the nanofluid was verified by visual inspection after ultrasonic agitation, and then immediately used.

Description of Experimental Technique

The system was moved to a laminar flow isolation optical bench, partially enclosed to prevent stray light from hitting the CCD. After this, the microfluidic chip was placed within the system and fixed within a particular position so that the focus of the diode lenses was on the channel chosen to be imaged. For each configuration of the system ('mirror', 'grating' and 'mirrorless'), the following procedure was then performed: 1) the same base EG used to produce the nanofluids was pumped through the system over a 10 minute period to remove the bulk of the remaining TiO_2 particles; 2) the laboratory's room lights were turned off to further reduce stray light; 3) the threshold frequency of the system was determined via use of the two-segment fit with power/current values taken in increments of 0.50mA for time-management purposes, with the current then raised until the intensity on the CCD reached a particular value which was then recorded, with each baseline intensity set to a similar value for all configurations of the system; 4) then, with a separate 1ml syringe to the one used for the EG previously, approximately 0.9ml of nanofluid was drawn from the 0.2% nanofluid, this syringe was then fixed within the syringe pump; 5) the syringe was manually pressed to remove the previous fluid from the system, and then the pump was turned on at a rate of 0.005ml/minute; 6) three sets of 1200 .tiff extension images were taken using the Allied Vision Vimba Viewer software; 7) then, the remaining nanofluid was returned to its respective container; 8) this process repeats further with each prepared concentration.

Description of Statistical Methods

The methodology for statistical analysis was informed by Hase Hughes [17]. To calculate the error on the percentage volume, the uncertainties due to the precision of the balance, ±0.1mg, was used. Data on the density of the Brookite TiO_2 was not provided on Sigma-Aldrich's data sheets. However a similar specification of Brookite provided by American Elements suggested a theoretical range of 4.08-4.18g/mL [23], meaning an uncertainty of ±0.05 was deemed appropriate. Then, using the uncertainty propagation equation provided by [17]:

$$\frac{\alpha_Z}{Z} = \sqrt{(\frac{\alpha_A}{A})^2 + (\frac{\alpha_B}{B})^2} \tag{2.2}$$

each uncertainty was propagated through to produce the uncertainty of the volumetric concentrations given by Equation 2.1.

The Central Limit theorem states that for any set of random variables with finite mean and variance, the sum of such will be normally distributed if the number of random variables is sufficiently large [17]. Therefore, as the number of measurements at each concentration meets this criteria, with three sets of 1200 intensity readings, the value of the intensity at a given concentration can be estimated as the mean, with uncertainty equal to the standard error as given by chapter 2 of Measurements and their uncertainties [17].

Due to the manual injection of fluid into the chip during the data collection process, the first set of 1200 images from each concentration was discarded, as there was an initially lower intensity due to the higher density of particles caused by high pressure compared to the pressure provided by the syringe pump itself.

To determine whether for a given concentration value there is a difference in the mean intensity, a *Z*-value statistical tests was used. Between each system, the null hypothesis of equal means and the alternative hypothesis of differing means will be tested. This test can be used between two independent random variables that are normally distributed, and can be used to determine the probability the means of the two variables are greater or lower through a one-tailed test, or if the means are

not equal [24]. A two-tailed test was used in this study to show that each system has an mean intensity of differing value at each concentration. The limitations of this test are two-fold.

First, it requires that the variables are independent [24], which should be true as the channels are cleaned throughout the experiments meaning the concentrations used from one experiment should not affect the next. The second issue is that although the test can show that two independent random variables have a differing mean, it does not demonstrate how much of an improvement one setup has over another - it will only demonstrate that there is a statistically significant improvement. This limitation however may not be an important consideration in this study, as this study attempts to demonstrate an improvement, not to evaluate how much of an improvement there is, which is reserved for future studies.

Post-processing of Noise

Within the use case of inline measurement of trace particle detection, the noise in the data must be taken into account. The ECDL's output stability varies depending how far above the threshold current the ECDL operates at. As described by [6], the sensitivity of an ECDL measurement increases close to threshold meaning that in order to detect small numbers of scatterers, the current should be brought down close to threshold. However as the ECDL is brought close to threshold, the noise due to the environment and quantum fluctuations increases. Figure 2.6 presents two background signals to demonstrate how with the same alignment, a lower current (and thus, a lower intensity) causes an increase in noise.
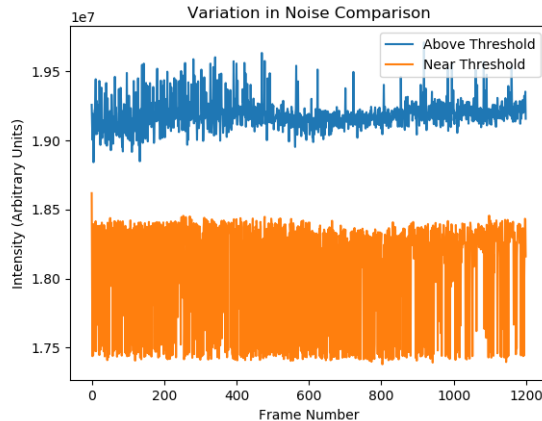
Figure 2.6: Graph comparing the noise of the ECDL's output when the current is near threshold and significantly above threshold.

Therefore, in order to detect low concentrations of scattering particles, a way of filtering the noise should be used so that an event of a scattering particle can be distinguished from the noise. Hence, three solutions to filtering the noise will be suggested.

Measurements and their Uncertainties [17] discusses the grouping of data into bins when demonstrating the definition of the standard error in section 2.7. This method can be used to adjust for random noise from a data set by binning adjacent data together and taking the mean as the value at the point mid way through the width of the bin. This method, however, requires a careful choice of bin size, as choosing bins too small will not sufficiently remove the noise, while choosing bins too large will make it difficult to spot discrete events. It is therefore arguable that in the case of scattering particles moving within the path of the ECDL beam that the average time taken for a particle to move through the beam should be used. Since the flow is laminar and the pump rate known, this is a reasonable quantity to determine for the use in measurements. With bins at this size, a particle event moving through the system will be represented by, on average, one or two data points, which can then be compared to a model of the background noise to determine the likelihood that an event occurred. Figure 2.7 demonstrates the difference between the filtered

and unfiltered background noise using this method, along with demonstrating the relative size of the errors in the mean.
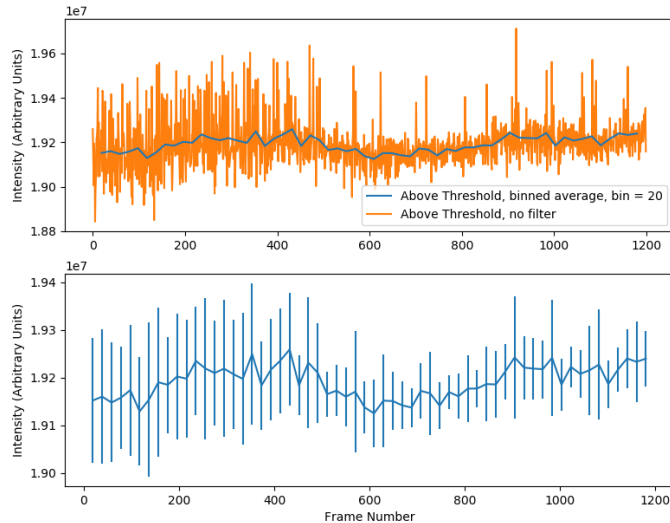
Figure 2.7: Comparison of Unfiltered background noise to adjacent binning of 'Above Threshold' data.

The moving/rolling average is another commonly used filtering method and is similar to the adjacent binning average described previously. The main difference is that instead of putting the data into bins, a window-width is specified. Each data point is replaced by the mean value of itself and a number of data points that come after it, with the user able to implement any value for this window. This method retains a lot more of the noise structure present in the previous method, but has the potential advantage of being less sensitive to the range size as opposed to the bin size of the previous method, allowing use in situations where the particle's velocity may not be as well known. To demonstrate this filter, Figure 2.8 compares the noise of the background data above threshold to its rolling average filtered counterpart.
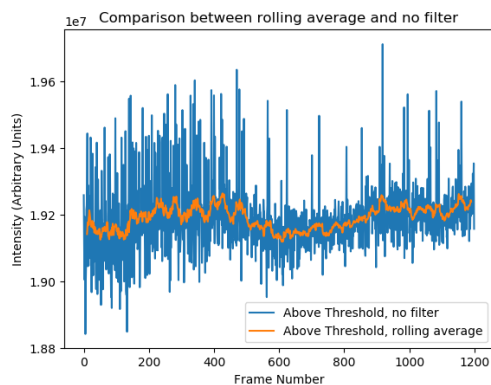
Figure 2.8: Comparison of Unfiltered background noise to rolling average of window-width 10 of 'Above Threshold' data.

Another method used often in analytical chemistry builds upon the moving average, and is known as the Savitzky-Golay filter [25]. This method takes a similar window specified in the moving average and instead fits a polynomial to the data within that range, via polynomial regression, with the new value being the value which corresponds to the x value at that point. As well as specifying a range, the degree of polynomial must also be chosen. This method allows for further preservation of that data's structure, which may allow it to be of use in cases with a relatively higher concentration of particles. Figure 2.9 demonstrates the use of this filter in a similar manner to the previous methods.
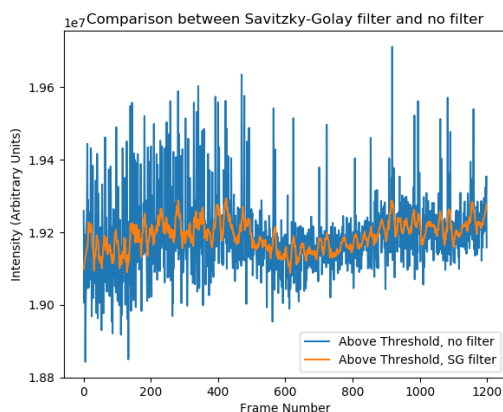
Figure 2.9: Comparison of Unfiltered background noise to Savitzky-Golay filter (window-width of 11, polynomial degree 2) of 'Above Threshold' data.

All of these methods are contingent on a bin or window width, which is required to be sufficiently large in order to reduce the uncertainty so that a particle measurement can be verified with statistical significance. However, the size of these quantities requires them to be similar to the time period that an image of a particle is within the CCD's sensor. Therefore, for purposes of inline, low particle count detection, it is required to both have a CCD which can perform relative to the velocities of the particles, and a sophisticated computer script to read off of the CCD's memory and store the information before it is lost. A final and important constraint to note for these methods is that the time between frames must be relatively consistent for these models to hold.

Results

This chapter will present the results of the study as figures and tables. Descriptions of the particular data sets will be given so that sufficient context with respect to the methodology described in chapter 2 can be established.

Experiment 1 - Volumetric Concentration/Intensity

The first set of data collected for intensity/concentration relationships using the methodology described in chapter 2 is presented by Figure 3.1.

Figure 3.1: A plot of the calibration curve of percentage volumetric concentration of the TiO_2 against the intensity profile of the ECDL for the three principle configurations of the system.

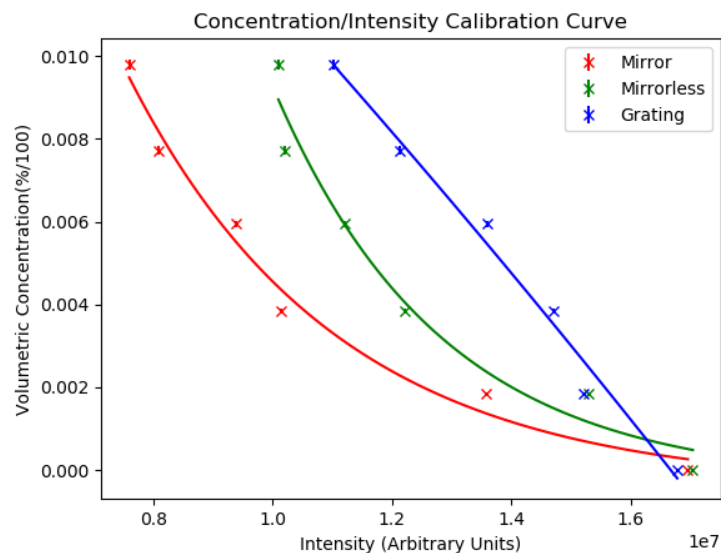| Measurements in Experiment 1			
	Intensity$\cdot 10^7$ (Arbitrary Units)		
Volumetric Concentration (%)	'Mirror'	'Mirrorless'	'Grating'
0	1.6952±0.0015	1.7035±0.0002	1.6774±0.0001
0.184±0.003	1.3569±0.0008	1.5290±0.0005	1.5206±0.0005
0.385±0.005	1.0146±0.0018	1.2205±0.0012	1.4698±0.0004
0.595±0.008	0.9383±0.0015	1.1208±0.0007	1.3584±0.0005
0.772±0.009	0.8088±0.0013	1.0208±0.0006	1.2119±0.0006
0.979±0.012	0.7597±0.0015	1.0096±0.0007	1.1027±0.0004
Reduced χ^2	355±1	992±1	5022±1

Table 3.1: Table of measurements and their uncertainties for Experiment 1.

The measured volumetric concentrations were found to be lower than the target volumetric concentrations, which are displayed in Tables 3.1 and 3.2.

The 'mirror' and 'mirrorless' setups were tested back to back with the 'mirror' system's data collected first, and the 'mirrorless' system's data collected second. The 'grating' setup's data was collected approximately 12 hours after the initial setups. As well as this, the position of the microfluidic chip was slightly adjusted for the collection for the 'grating' setup. The reduced chi-squared values are presented in Table 3.1, along with the intensity/concentration measurements and their uncertainties. A reduced chi-squared fitting linear-regression method was used to estimate an exponential relationship, given by the line of best fits. Since the uncertainties on the intensity values was low due to the volume of measurements, the uncertainty on the independent variable, volume concentration, was used, and because of the low uncertainty on the intensity, a total regression model was decided against.

To test the null hypothesis of whether the 'mirrorless' setup's mean intensity is the same as the 'mirror' setup, two tailed Z-value tests were performed at each concentration value. Figure 3.2 shows the result of this test.
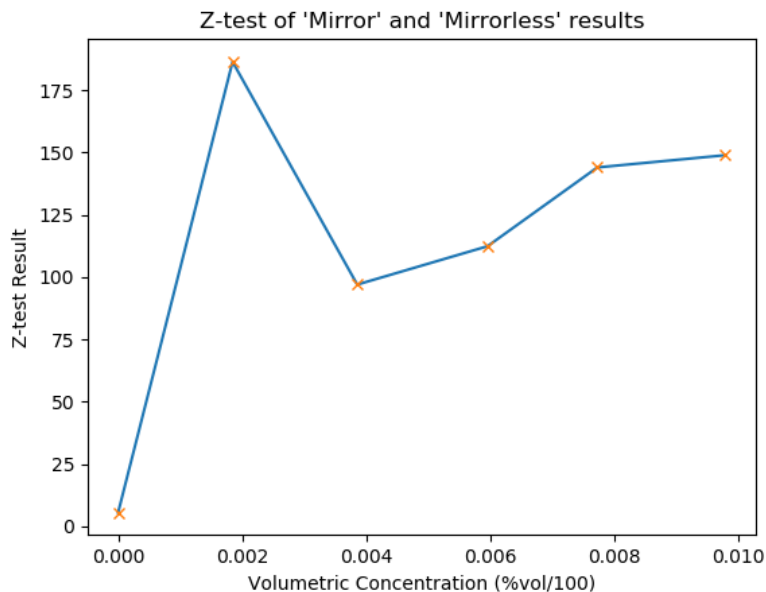
Figure 3.2: *Z*-tests of Experiment 1 data between the 'mirror' and 'mirrorless' setups at each concentration.

Experiment 2 - Volumetric Concentration/Intensity

A second experiment was conducted using the same methodology as Experiment 1, with the addition of a 1.143% volumetric concentration sample to observe if the ECDL system would continue the behaviour displayed in Experiment 1. Both setups were calibrated to have a similar threshold frequency as the ones used in Experiment 1. In this experiment the 'grating' data and the 'mirror' data were collected immediately after the other was completed to minimise the time delay and avoid any realignment. These results are displayed in Figure 3.3 with corresponding numerical values and their uncertainties presented in Table 3.2.

'Mirrorless' data was unable to be produced within a similar time frame, and due to the incongruence of the 'grating' data in Experiment 1, it was decided that this system configuration of the system would not be tested. Instead, a comparison of two similar alignments of the microfluidic chip within the 'mirror' system was used to investigate the extent to which a small change in the alignment would affect this type of calibration measurements, given in Figure 3.4.
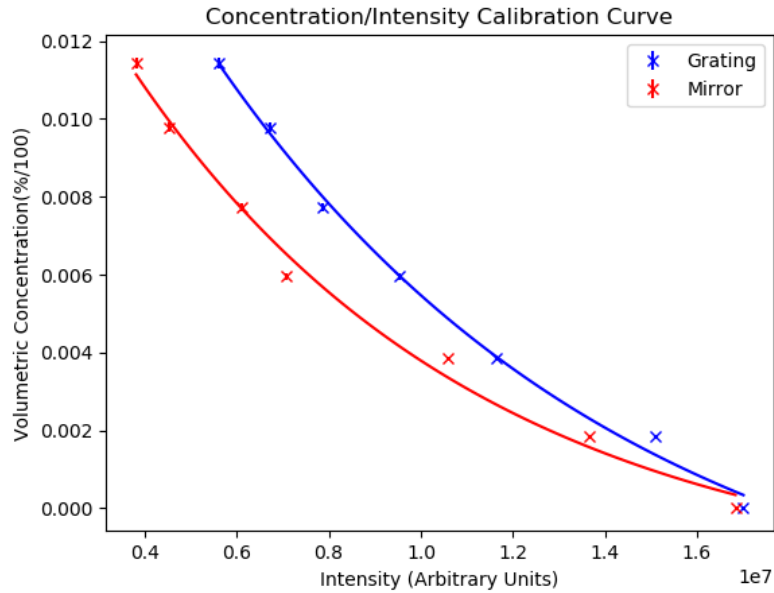
Figure 3.3: A plot of the calibration curve of percentage volumetric concentration of the TiO$_2$ against the intensity profile of the ECDL for the two ECDL configurations of the system.

Measurements in Experiment 2		
	Intensity·10^7 (Arbitrary Units)	
Volumetric Concentration (%)	'Mirror'	'Grating'
0	1.6952±0.0015	1.7035±0.0002
0.184±0.003	1.3662±0.0012	1.5101±0.0017
0.385±0.005	1.0577±0.0010	1.1638±0.0008
0.595±0.008	0.7085±0.0016	0.9526±0.0013
0.772±0.009	0.6100±0.0012	0.7878±0.0025
0.979±0.012	0.4530±0.0008	0.6730±0.0008
1.143±0.014	0.3813±0.0009	0.5611±0.0010
Reduced χ^2	351±1	345±1

Table 3.2: Table of measurements and their uncertainties for Experiment 2.

Similar to Experiment 1, to test the null hypothesis of the 'mirror' setup having a different mean value than the 'grating' setup at each concentration value, Z-value statistic tests were used, with the results shown in Figure 3.5.
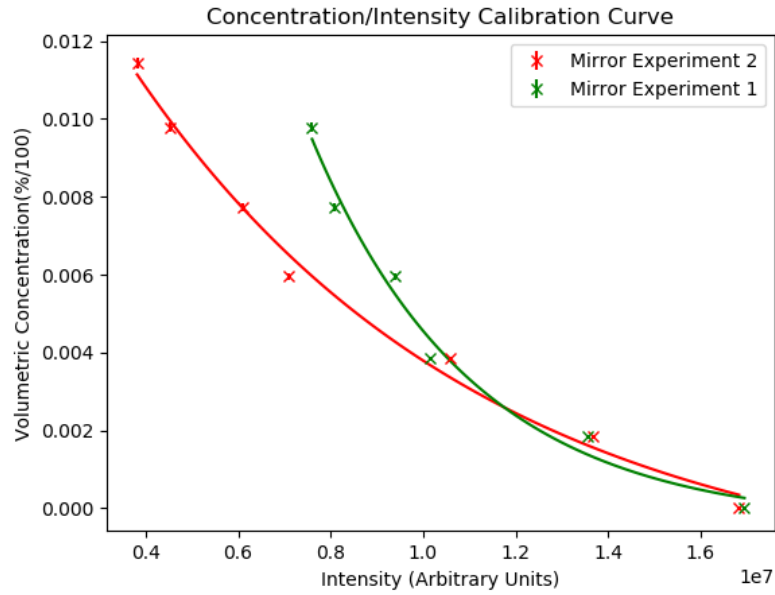
Figure 3.4: Plot of the 'mirror' system's Volumetric Concentration/Intensity relationships, with differing alignments between the measurements taken in Experiments 1 and 2.
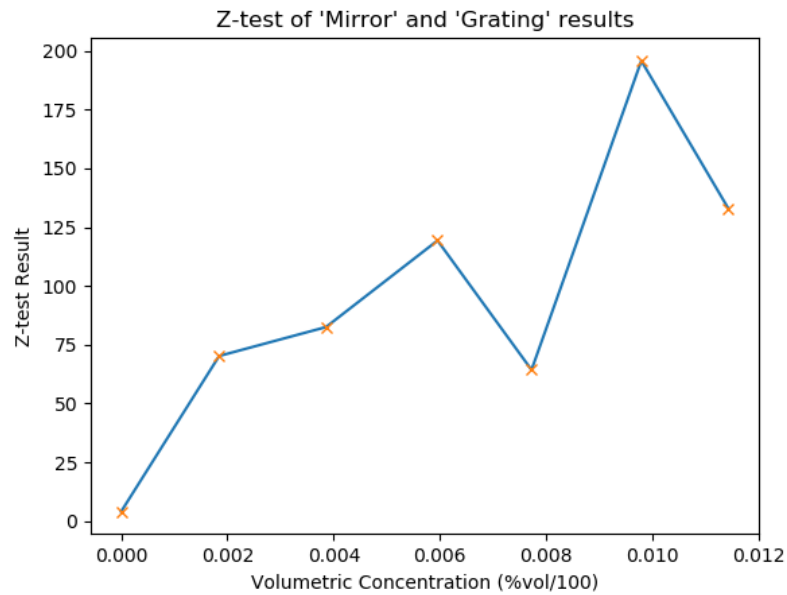
Figure 3.5: *Z*-tests of Experiment 2 data between the 'mirror' and 'grating' setups for each concentration.

Experiment 3 - Low Concentration of Scatterers

In order to investigate the capabilities of the system for continuous inline measurements of low concentrations of scatterers, EG was pumped through the channels to remove the excess nanofluid after the first two experiments had concluded. Then, once the number of particles seen passing through the system sufficiently low as determined via manual inspection, intensity images were taken. Figure 3.6 displays the unfiltered intensity along with the three noise-reducing methods discussed in chapter 2, with a bin/window size of 3.
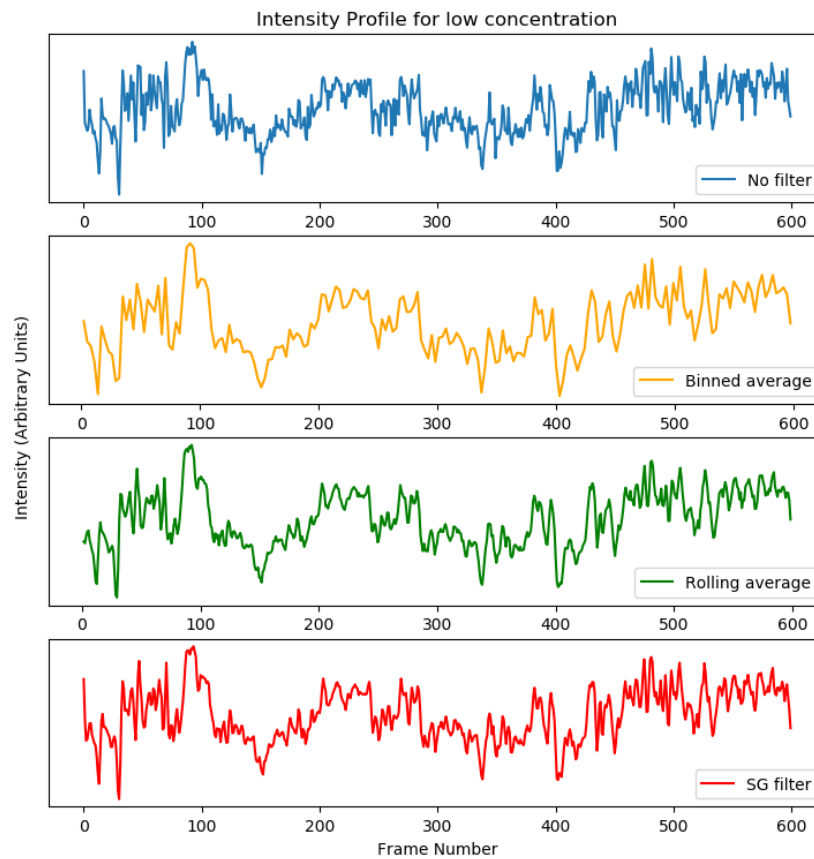
Figure 3.6: A plot of a continuous intensity profile, taken while trace scatterers pass through the microfluidic channel, with each noise filter applied with a bin/window size of 3.

To summarise this chapter, the primary results of the study are presented by Experiment 1 and Experiment 2, with their implications discussed in chapter 4. On the other hand, Experiment 3 was inconclusive due to limitations in the software used with the CCD, which is also described in chapter 4.

Discussion

This chapter will start by noting points of interest discovered during the acquisition of results which may be of note for similar future experiments. This will lead to a discussion of the figures presented in chapter 3, including interpretation of trends and their implications on potential use cases of the ECDL. The statistical analyses mentioned in chapter 2 will be referenced and used to justify inferences made.

Post-Experimental Considerations

Although the intention of this study was to use the setup without a reflective element as a null hypothesis, there is an important phenomenon to note. Some of the optics used in the setup while functioning in the near-infrared, were not optimized for the specific wavelength of the laser diode used. Because of this, there was a significant level of reflection back into the diode's gain material even without an reflective element intentionally placed within the system, providing a minor contribution to cavity effects and producing some external cavity operation. The diode lenses used to focus the beam were particularly problematic in this regard. However, due to a large proportion of this reflected light diverging, only a small amount of light contributed to these effects, and so only a small amount of external cavity effects were present. Given that this setup was used to present a lower finesse cavity, this setup still performed its function as intended.

Discussion of Experiment 1

The set of data yielded by Figure 3.1 demonstrates several key points. The apparent incongruence between the 'mirror' and 'mirrorless' systems compared with the 'grating' setup highlighted the importance of taking the data in a similar time frame and for the system to not be adjusted, as the change in the position of the chip along the Z axis likely changed the volume of scattering particles being imaged, and along with the potential difference in concentrations of the nanofluids due to agglomeration, this may have led to the 'grating' setup's intensity/concentration profile being weaker compared to the baseline 'mirrorless' setup, prompting a further set of data to be required.

The Z-value tests presented in 3.2 are contingent on the values of the independent variable, volumetric concentration, being sufficiently similar. While this is in question, under the condition that this is true, the Z-value tests show that there is a statistically significant difference between the 'mirror' and 'mirrorless' setups above the 5σ confidence level. This is an important result, as even if the number of data points is insufficient to demonstrate an exponential relationship for the calibration curve, it does show that there is a significant advantage in the 'mirror' setup, as a lower intensity value at a given concentration allows for higher sensitivity when used as a measuring device compared to the standard diode setup.

One of the unexpected features presented by Figure 3.1 is related to the gradient. In the case of the 'mirrorless' setup, the difference in intensity between 0.8% and 1.0% volume concentrations was small. Although they were not within the error of one another, there is a reduced sensitivity in this range due to the intensity not varying as much. In comparison, in the 'mirror' setup, there is still a large change in intensity value. This could suggest that the ECDL setup presents not only a potential higher sensitivity for measurement, but also a higher dynamic range, allowing for a larger range of concentrations to be calibrated for.

Discussion of Experiment 2

Results from Figure 3.1 were used as a case study for the subsequent data set collected in Figure 3.3 in terms of procedure, as the need for consistency in alignment and the time of data collection were crucial for this experiment.

Figure 3.3 demonstrates that despite the unique filtering properties of the 'grating' setup, there is a similar relationship between the systems, with the 'mirror' system having a lower intensity at each volume and the separation between the mean intensities between the two increasing at higher concentrations. This would suggest with similar uncertainties on the intensity measurements that the 'mirror' setup has a greater improvement, which may be due to having a higher reflectivity and therefore a higher finesse cavity, similar to that demonstrated in Figure 3.1. Although a direct comparison between this data and the 'mirrorless' data from Figure 3.1 can not be achieved, the fact that the intensity relationship continues at higher concentrations similar to the 'mirror' setup in Figure 3.1 suggests that there may be a continuation of the higher dynamic range observed in the previous experiment. This is particularly beneficial, as in the application of the ECDL as a measurement apparatus, improved dynamic range allows the device to be used in more circumstances.

Finally, similar to the discussion for Experiment 1, the Z-value statistic hypothesis tests shown in Figure 3.5 demonstrated that under the condition that the concentration being measured is the same, there is a statistically significant difference between the mean intensity measured at each respective value of concentration above the 5σ level. This means it can be said that there is a benefit in the 'mirror' setup compared to the 'grating' for the concentration/intensity relationship, which is likely due to the increased finesse of the cavity in the 'mirror' setup.

Intensity profile variation between experiments

The effect on intensity that two differing alignments can have is shown in Figure 3.4. Both data sets have a similar initial relationship at lower concentrations, but as the concentration increases they begin to diverge. This could be due to the change in alignment causing the ECDL's beam to be focused on a different sized cross section on the microfluidic chip, which would mean a different volume of scattering is being sampled from. Another reason, which may change the density of scattering particles, is differences in the nanofluids used. Although samples were drawn from the same storage containers for each experiment, the nanofluids for Experiment 2 were sonicated again for 5 hours, due to agglomeration. Since this was carried out after the 5 hours of sonication done for Experiment 1, there may have been an average smaller agglomerations in the nanofluids in Experiment 2, benefiting from both sonication sessions. With a smaller agglomeration size, the nanofluid may have a differing density, contributing to a difference in scattering cross-sections measured. It is likely that both of these contributed to the differences seen in Figure 3.4, and so both should be controlled for. To control for the alignment, a way of recording the position of the chip should be used, and ideally any time the orientation of the chip is changed with respect to the ECDL, new calibration curves should be calculated. The application will determine the methodology required to control for the scattering cross-section, as there will be significantly different factors used than those with TiO_2 nanofluids.

Comparison of reduced χ^2 values

The reduced chi-squared values in Experiment 1 on the fitting of the exponential model of the 'mirror' set of $\chi^2_{mirror} = 355$ and $\chi^2_{mirrorless} = 992$ have two main interpretations.

The first concept is that the uncertainties on the concentration of the TiO_2 nanofluids are underestimated. Three factors could contribute to this. The error due to TiO_2 and EG being lost during transferal to the same container is a likely can-

didate. However, estimation of this is not possible post-hoc, as it would require systematically measuring the mass of containers multiple times during the process of combination to determine the mass of each reagent remaining after transferal. This is something which can be implemented in future studies to minimise this error. Another contributing factor could be the measuring balance used, as the calibration was not verified and a data sheet could not be found with the relevant manufacturer calibration data. Finally, the concentration of the nanofluid once it is in the system could be responsible, as it is possible that the concentration within the system varies in a non-linear manner with respect to the original concentration as it is pumped through the system.

The second possible reason why the χ^2 value may be so high is that the model used may not be appropriate. This would mean that a data set with a larger sample of concentration values would be required, and potentially a different fitting method to approximate the relationship instead of an exponential fit. Increasing the maximum value of the concentration range would be difficult beyond a certain point, as higher concentrations lead to a higher rate of agglomeration of the nanofluid. However, between the already set range it would be suitable to take measurements, as long as the balances used to measure weight had sufficient precision.

Reduced χ^2 values for Experiment 2 of $\chi^2_{mirror} = 351$ and $\chi^2_{mirror} = 345$ are similar in magnitude to the fitting of the 'mirror' setup in Experiment 1. This is of interest, as it suggests that the exponential fitting used during linear regression is an appropriate approximation, with a systematic underestimation of errors contributing to a similar reduced χ^2 value. However, it is possible that an exponential fit is not appropriate for the 'mirrorless' setup in Experiment 1, with approximately three times the reduced χ^2 value. This may be of interest for further investigation in a future study.

Significance of fitting to Theory

In chapter 1, both Rayleigh and Mie scattering were discussed as possible candidates for scattering interactions. Although initially it was proposed that Rayleigh scattering would dominate due to the nanoparticle diameters rated as <100nm [26] by the manufacturer, the exponential fittings used, if correct, may suggest that the Mie scattering regime described by equations 1.6 and 1.7 may be dominant. This would suggest that the agglomerations of nanoparticles are of a similar size to the wavelength used of 808nm. The systematic testing of the variation of the scattering profile as the particle size is decreased is a possible route of exploration for future studies, although this would require a method of verifying the nanoparticle size.

Discussion of Experiment 3

Experiment 3 highlighted one of the major equipment and software issues experienced during the study. As images were taken with the CCD, although the CCD while in free run mode can record images at 90 frames per second, when the Vimba Viewer Allied Vision software attempted to save a set of images, approximately 83% of images were lost. Not only did this mean that the CCD was operating at an average of 15 frames per second, it meant that the time between frames was not continuous. This made it difficult to justify a large time bin for the purposes of filtering as described in chapter 2, as it was found by manual inspection that particles would remain in the recorded images between 1 and 3 frames. Even with the larger window size of 3, it is still not enough to discern events from the noise. Therefore, it was a challenge to pair changes in the intensity profile with particle events as the decrease in intensity can be less than the changes caused by fluctuations. This is less of a problem when more images are acquired for a single particle's presence as described in chapter 2, and is why the data in Experiments 1 and 2 are designed to not be contingent on the frame rate's size or consistency. By manual inspection, some of the noise appeared to have a consistent frequency. It is possible that this noise was due to the frequency at which the stepper motor which drives the syringe

pump operates at, adding noise in intensity at regular intervals. This suggests that the use of a Fourier transform frequency filter may be useful with a data set with a consistent frame rate to remove this consistent noise, and potentially could be used to remove the random noise due to fluctuations in threshold frequency caused by the environment.

Conclusion

The conclusion of chapter 1 stated the primary aims of the study: to measure concentration/intensity profiles to demonstrate a benefit of an ECDL system in comparison to the output of a standard laser diode for the purposes of scattering based microscopy measurements. This chapter will close the study by evaluating the extent to which this has been demonstrated this, along with noting important questions left unanswered by this study for future projects to investigate.

Summary of Findings

The results presented, while not being from a single comprehensive, directly comparable data set, show that there is a lower intensity for a given concentration using a highly reflective mirror when compared with the control. This improvement may also apply to a blazed reflective grating as a reflected element, although more evidence using a similar methodology to those used in Experiment 2 is required to confirm this. However, for a blazed diffraction grating, the reduced average efficiency of 60% compared to the mirror's 98% reflectivity will likely leave it not as optimal for this purpose as a highly reflective mirror. Data collected using both a highly reflective mirror and blazed reflective diffraction grating suggests that there may be an improvement in dynamic range compared with a standard laser diode's output, which is of general interest for any use case in which the ECDL is used as a calibrated measuring device.

Due to the high values of χ^2, the study was unable to determine whether an exponential relationship was observed, and therefore a conclusion on whether Mie or Rayleigh scattering is dominant cannot be made. The use of a microfluidic system along with the method used in the production of the TiO_2 nanofluid suggested that there was a large systematic underestimation of the error on the volumetric concentration, meaning that while an exponential fit could be appropriate, it is by no means conclusive. However the more simplistic Z-value statistic test presented compelling verification that the measured concentration/intensity curves were significantly different.

Due to difficulties in obtaining both consistent and high frame rates, this study was unable to thoroughly investigate inline methods of low concentration light-scattering particle detection, although potential methodology for future studies to utilise is given.

Potential Investigations beyond this study

Routes of further investigation beyond this study have several options.

There may be a need for further exploration on how much of an improvement on the dynamic range can be made, as this was an unexpected improvement observed which the study was not designed to investigate. Further confirmation of the relationships seen, with higher concentrations of scatterers may be appropriate.

Investigation of the relationship between the finesse of the cavity and the concentration/intensity relationships is of interest as this was not varied in a manner to determine to what extent the reflective element's reflectivity is important. Studies in the future may possibly look towards investigation of an optimal value of reflectivity for differing use cases, as there may be a trade-off between improved precision and the size of the improvement on the dynamic range.

On the investigation of use cases, the demonstration of similar relationships in situ with a focused flow droplet generator microfluidic system may be of interest

to verify whether the nanofluid scattering model applies in the case of droplets in these microfluidic chips. For use in microfluidic based cytometry, there will need to be verification of the utility of the low concentration scattering detection methodology attempted during this study.

Bibliography

[1] M. Kanskar et al. 73% cw power conversion efficiency at 50w from 970nm diode laser bars. *Electronics Letters*, 41:245–247(2), March 2005.

[2] D. P. Kapasi, J. Eichholz, T. McRae, R. L. Ward, B. J. J. Slagmolen, S. Legge, K. S. Hardman, P. A. Altin, and D. E. McClelland. Tunable narrow-linewidth laser at 2μm wavelength for gravitational wave detector research. *Opt. Express*, 28(3):3280–3288, Feb 2020.

[3] D W Hughes and J R M Barr. Laser diode pumped solid state lasers. *Journal of Physics D: Applied Physics*, 25(4):563–586, apr 1992.

[4] J. O. Akinlami and A. O. Ashamu. Optical properties of GaAs. *Journal of Semiconductors*, 34(3):032002, mar 2013.

[5] W. Demtröder. Laser Spectroscopy Basic Concepts and Instrumentation. 2003.

[6] Untzizu Elejalde and John M. Girkin. Real-time, ultralow concentration detection of analytes in solution by infrared intracavity laser absorption. *Appl. Opt.*, 46(19):3995–3999, Jul 2007.

[7] Paul Lee Gourley, Ken E. Meissner, Thomas M. Brennan, B. Eugene Hammons, and Mark F. Gourley M.D. Surface-emitting semiconductor laser spectroscopy and microscopy for characterizing normal and sickled red blood cells.

In Robert R. Alfano, editor, *Advances in Laser and Light Spectroscopy to Diagnose Cancer and Other Diseases II*, volume 2387, pages 148 – 161. International Society for Optics and Photonics, SPIE, 1995.

[8] David J. Lockwood. *Rayleigh and Mie Scattering*, pages 1097–1107. Springer New York, New York, NY, 2016.

[9] P L Gourley. Biocavity laser for high-speed cell and tumour biology. *Journal of Physics D: Applied Physics*, 36(14):R228–R239, jul 2003.

[10] James. Hicks and Gabor. Patonay. Linearity considerations for a near-infrared laser diode intracavity absorption spectrophotometer. *Analytical Chemistry*, 62(14):1543–1545, 1990.

[11] Marco PC Marques and Nicolas Szita. Bioprocess microfluidics: applying microfluidic devices for bioprocessing. *Current Opinion in Chemical Engineering*, 18:61 – 68, 2017. Biotechnology and bioprocess engineering / Process systems engineering.

[12] Micronit Micro Technologies B.V. A guide to droplet generation. Retrieved 2021.

[13] L. Ricci, M. Weidemüller, T. Esslinger, A. Hemmerich, C. Zimmermann, V. Vuletic, W. König, and T.W. Hänsch. A compact grating-stabilized diode laser system for atomic physics. *Optics Communications*, 117(5):541 – 549, 1995.

[14] D. M. Kane and Joshua P. Toomey. Precision threshold current measurement for semiconductor lasers based on relaxation oscillation frequency. *Journal of Lightwave Technology*, 27(15):2949–2952, 2009.

[15] Tyll Hertsens. An overview of laser diode characteristics. 2005.

[16] Hans Petter Langtangen. Truncation Error Analysis. 15/10/2015.

[17] Ifan Hughes and Thomas Hase. Measurements and their uncertainties. a practical guide to modern error analysis. 07 2010.

[18] Mohd Hazrie Samat, Mohamad Fariz Mohamad Taib, Oskar Hasdinor Hassan, Muhd Zu Azhan Yahya, and Ab Malik Marwan Ali. Structural, electronic and optical properties of brookite phase titanium dioxide. 2017.

[19] Sigma-Aldrich. Titanium(IV) Oxide, Brookite Nanopowder Saftey Data Sheet, https://www.sigmaaldrich.com/GB/en/sds/aldrich/79132. Retrieved 2021.

[20] Liu Yang and Yuhan Hu. Toward tio2 nanofluids—part 1: Preparation and properties. *Nanoscale Research Letters*, 12, 06 2017.

[21] Abu Ali and Bodius Salam. A review on nanofluid: preparation, stability, thermophysical properties, heat transfer characteristics and application. *SN Applied Sciences*, 2:1636, 10 2020.

[22] Wei Yu and Huaqing Xie. A review on nanofluids: Preparation, stability mechanisms, and applications. *J. Nanomaterials*, 2012, January 2012.

[23] American Elements. Titanium(IV) Oxide, Brookite Nanopowder, https://www.americanelements.com/titanium-iv-oxide-brookite-nanopowder-12188-41-9. Retrieved 2021.

[24] David Lane. Introduction to statistics. 2003.

[25] Abraham. Savitzky and M. J. E. Golay. Smoothing and differentiation of data by simplified least squares procedures. *Analytical Chemistry*, 36(8):1627–1639, 1964.

[26] Sigma-Aldrich. Titanium(IV) Oxide, Brookite Nanopowder, https://www.sigmaaldrich.com/GB/en/product/aldrich/791326?context=product. Retrieved 2021.

Colophon

This thesis is based on a template developed by Matthew Townson and Andrew Reeves. It was typeset with LaTeX 2_{ε}. It was created using the *memoir* package, maintained by Lars Madsen, with the *madsen* chapter style. The font used is Latin Modern, derived from fonts designed by Donald E. Kunith.